Resonance Raman spectra of an O₂-binding H-NOX domain reveal heme relaxation upon mutation[†]

Rosalie Tran[‡], **Elizabeth M. Boon[‡,⊥]**, **Michael A. Marletta[‡,§,*]**, and **Richard A. Mathies[‡,*]**

[‡]Department of Chemistry, University of California, Berkeley, CA 94720

[§]Department of Molecular and Cell Biology, University of California, Berkeley, CA 94720

Abstract

Resonance Raman spectra are measured for *Tt* H-NOX WT and three other *Tt* H-NOX proteins containing mutations at key conserved residues to determine the heme conformation in solution. The most dramatic changes in heme conformation occurred in the O₂-bound forms, and the single *Tt* H-NOX P115A mutation was sufficient to generate a significant relaxation of the chromophore. Clear evidence of heme relaxation in the *Tt* H-NOX I5L, P115A, and I5L/P115A mutants in solution is demonstrated by the observation of reduced resonance Raman intensities for several out-of-plane low frequency modes (*e.g.* γ_{11}, γ_{12}, γ_{13}, and γ_{15}) in the 400–750 cm^{-1} region known to be sensitive to ruffling and saddling deformations, as well as increased vibrational frequencies for the core heme skeletal stretching modes, ν_3, ν_2, and ν_{10}. In addition, all three mutants exhibited some degree of heme conformational heterogeneity based on several broad skeletal markers (*e.g.* ν_{10}) in the high frequency region. These results are comparable to those observed by Olea *et al.* for *Tt* H-NOX P115A in crystal form, where four different heme structures were determined from a single unit cell. Based on the resonance Raman spectra, it is clear that the actual heme conformation for *Tt* H-NOX P115A in solution is considerably more relaxed than WT, with increased flexibility within the protein pocket, allowing for rapid sampling of alternate conformations.

Keywords

Resonance Raman spectroscopy; H-NOX; *Thermoanaerobacter tengcongensis*; porphyrin distortion; vibrational analysis; normal coordinate structural decomposition (NSD); O₂ binding

Nonplanar porphyrin conformations are of great interest and widely investigated due to their potential role in regulating biochemical properties and activity in proteins containing either heme or chlorophyll cofactors (1–7). Over the last three decades, several methods have been utilized to study these heme deformations in proteins. These include theoretical approaches using DFT and QM/MM methodologies (2,6,8,9), vibrational spectroscopy of model compounds isolating specific distortions (3,5,10–12), and the normal coordinate structural decomposition (NSD) method developed by Shelnutt *et al.* (4,7,13) to quantify specific heme

deformations observed in x-ray crystal structures. In nature, some of the largest heme deformations typically occur in the c-type cytochromes and peroxidases with out-of-plane displacements greater than 1 Å (7). However, recent crystallographic work by Pellicena *et al.* shows that the *H*eme-*N*itric oxide and/or *OX*ygen binding (H-NOX) domain from *Thermoanaerobacter tengcongensis* also contains a highly distorted heme structure (14). Subsequent H-NOX crystal structures indicate that the heme chromophore can sample a range of nonplanar conformations (15,16).

The H-NOX family of heme proteins has the unique property that some proteins bind only NO and CO, whereas others additionally bind O_2 (17,18). The first crystal structure obtained within this family was the O_2-bound H-NOX domain from the bacterial obligate anaerobe, *Thermoanaerobacter tengcongensis* (*Tt* H-NOX) (14). One of the most distinctive features about this O_2-bound structure is the significant heme deformation (Figure 1a). Energy minimization calculations by Pellicena *et al.* predicted that Ile-5, Pro-115, and Leu-144 maintained nonbonded contacts with the heme, inducing this observed deformation in *Tt* H-NOX (14,19). Of those three residues, Pro-115 is of particular interest since it is conserved within this family. Thus, a key focus in investigating these H-NOX domains is to better understand how these conserved residues may contribute towards regulating heme distortion, and thereby possibly controlling ligand specificity.

Recently, Olea *et al.* have shown via x-ray crystallography that mutating Pro-115 to alanine in *Tt* H-NOX alters the protein pocket such that the heme relaxes and samples several conformations, including more planar structures than that observed in the WT protein (20). However, the presence of four different heme structures in the unit cell complicated the determination of which conformation is actually dominant in solution. To address this question, a different technique that can probe the heme structure in solution is required.

Because of its selectivity and sensitivity to molecular structure, resonance Raman spectroscopy is an invaluable tool for specifically probing protein-bound heme conformations in solution (Figure 1b). Detailed information on the ground state geometry and electronic structure can be obtained from the vibrational frequencies; furthermore, the RR intensities provide insight into the symmetry and equilibrium geometry, and may be used to probe excited state dynamics (21, 22). In addition, RR spectroscopy is useful for investigating heme deformations because the distortions within the chromophore cause frequency shifts in the skeletal stretching modes (denoted as "ν") and activate the intensity of low frequency out-of-plane (oop) modes (denoted as "γ") (5, 7, 21, 23).

In this study, we use resonance Raman spectroscopy to investigate the effects of mutating the distal Ile-5 and proximal Pro-115 residues in *Tt* H-NOX on the heme structure. The spectra show that these residues are important in *Tt* H-NOX for maintaining a specific protein environment, and that mutating Ile-5 and Pro-115 relaxes the solution chromophore conformation for the O_2 complexes. Specifically, our RR spectra suggest that the single P115A mutation leads to the largest change in the heme structure, whereas the *Tt* H-NOX I5L and I5L/P115A double mutants maintain conformations that are more similar to *Tt* H-NOX WT. These conformational changes likely occur as a consequence of heme pocket rearrangements to accommodate the substituted residues. We compare these relaxations to the quantified changes observed in crystal form using the normal coordinate structural decomposition (NSD) analysis developed by Shelnutt *et al.* (4,7,11,13).

MATERIALS AND METHODS

Protein expression and purification

Expression and purification of the *Tt* H-NOX domain were performed as previously described (19) with the following modifications. Thawed cell pellets resuspended in buffer A [50 mM TEA, 20 mM NaCl, 5% glycerol, 1 mM Pefabloc (Pentapharm), pH 7.5] were lysed at 4 °C with an Emulsiflex-C5 high-pressure homogenizer at 15000 psi (Avestin, Inc.) upon addition of DNAse I and lysozyme (Sigma). Lysed cells were centrifuged for 1 h at 42000 rpm at 4 °C, and the supernatant was heat-denatured at 75 °C for 45 min. The denatured protein was centrifuged again for 1 h at 42000 rpm, and the supernatant was concentrated to < 10 mL using 10 K MWCO spin concentrators (Vivaspin). Concentrated protein was then loaded onto a prepacked Superdex S75 Hiload 26/60 gel filtration column (Pharmacia) equilibrated with buffer A, and fractions containing *Tt* H-NOX were pooled and applied to a POROS HQ 7.9 mL (1×10 cm, 10 µm) anion-exchange column (Applied Biosystems) at 5–10 mL/min. Flow-through containing the *Tt* H-NOX domain was collected and stored at −80 °C. Site-directed mutagenesis was carried out using the QuikChange® protocol (Stratagene), and verified by sequencing (UC Berkeley sequencing core).

Sample preparation

The purified *Tt* H-NOX protein was brought into an anaerobic glovebag, and oxidized using ~5–10 mM potassium ferricyanide to remove the bound O_2. The ferricyanide was removed using a PD10 desalting column (Amersham Biosciences) equilibrated with buffer B (50 mM TEA, 50 mM NaCl, pH 7.5). Following oxidation and desalting, the protein was reduced with ~5–20 mM sodium dithionite that was removed using a PD10 desalting column upon complete reduction of the heme. The $^{16}O_2$ complexes were generated by opening the reduced protein to air. To make the $^{18}O_2$ (95% $^{18}O_2$; Cambridge Isotopes) complexes, gas was added to a sealed Reacti-Vial (Pierce) containing Fe^{II}-unligated protein. Commercially available horse heart myoglobin and horse muscle hemoglobin (Sigma) samples were prepared similarly. Final sample concentrations for the Raman experiments were typically 15 to 50 µM. All UV/Vis absorption samples were prepared and measured as previously described (19,24).

Resonance Raman spectroscopy

All spectra were collected using the 413.1 nm line from a Kr^+ laser (Spectra-Physics model 2025) focused to a beam diameter of ~60 µm with a 50 mm focal-length excitation lens. Raman scattering was detected with a cooled, back-illuminated CCD (LN/CCD-1100/PB; Roper Scientific) controlled by an ST-133 controller coupled to a subtractive dispersion double spectrograph (25). The laser power at the sample was ~2 mW, and a microspinning sample cell was used to minimize photoinduced degradation. Typical data acquisition times were 30 to 60 min. Electronic absorption spectra were obtained before and after the Raman experiments to verify that no photoinduced degradation occurred. Raman spectra were corrected for wavelength dependence of the spectrometer efficiency with a white lamp, and the instrument was calibrated using the Raman frequencies from cyclohexane, CCl_4, and toluene. The reported frequencies are accurate to ± 1 cm^{-1}, and the spectral bandpass was set to 8 cm^{-1}. For each Raman spectrum, the raw data were baseline-corrected, and the buffer background signal was subtracted. Spectral analysis and decomposition were performed using Igor Pro (WaveMetrics). Isotopic shifts were approximated on the basis of a simple harmonic oscillator (HO) model.

Structural deformation analysis

To deconvolute the distortions from *Tt* H-NOX and other heme proteins, we used the web-based version of the normal-coordinate structural decomposition method (NSD) developed by

Jentzen *et al.* to input our heme coordinates and quantify the deformations for the porphyrin macrocycle (4,7,11,13). This program uses a porphyrin reference of D_{4h}-symmetry to describe the heme distortions in terms of displacements along the lowest frequency out-of-plane normal coordinates within the molecule. The generated output quantifies the amount of each deformation type necessary to model the overall observed distortions within a given heme structure. Coordinates from previous crystal structures were obtained from the RCSB Protein Data Bank (14,20,26–29). For all proteins used in our NSD calculations, the heme is oriented such that the vinyl groups remain in quadrants I and II as defined by Jentzen *et al.* (4) in order to maintain the directionality in the absolute signs of the deformation types. In our analysis, the minimal basis set was used to quantify the different types of heme distortion. This basis set only includes the lowest frequency mode from each of the 6 in-plane and 6 out-of-plane normal deformations, and has been shown to adequately describe heme distortions in proteins (13). The overall magnitude of out-of-plane distortions (Δ_{oop}) for the heme is defined as the square root of the squared sum of observed z axis displacements for the 24-atom porphyrin macrocycle ($C_{20}N_4$). This total out-of-plane distortion was determined from the complete basis set, which gives the total deformation of each symmetry type (13).

RESULTS

Electronic absorption characterization

As an initial step toward characterizing the effects of mutating Ile-5 and Pro-115 in *Tt* H-NOX, we obtained electronic absorption spectra of the proteins with different ligands. Table 1 summarizes the Soret and α/β bands measured for *Tt* H-NOX in the unligated, CO, NO, and O_2-bound forms, and includes the globins for comparison (30).

Both the unligated and CO complexes show small changes in absorption upon mutating Ile-5 and Pro-115. The unligated *Tt* H-NOX WT spectrum displays a characteristic Soret at ~430 nm and a broad α/β band at ~563 nm, indicative of a 5-coordinate, high-spin species. Compared to *Tt* H-NOX WT, the P115A, I5L, and I5L/P115A mutants produce minor red shifts between 1–6 nm in the Soret and α/β bands. Addition of CO to the reduced, unligated *Tt* H-NOX WT protein shifts the electronic absorption features to display the Soret at ~423 nm and discernible α/β bands at ~567 nm and ~541 nm, confirming the presence of a 6-coordinate, low-spin CO complex. All three *Tt* H-NOX mutants display similar Soret values at 424 nm, but deviate by 1–3 nm in the split α/β band region compared to *Tt* H-NOX WT.

Addition of NO to the reduced, unligated *Tt* H-NOX WT protein results in a 6-coordinate, low-spin NO complex (Soret: 420 nm, α/β bands: 575 nm and 547 nm). A slight blue shift of 2–4 nm is observed in the Soret and α/β bands for the *Tt* H-NOX P115A NO complex. Although the Soret only shifts to 421 nm for the *Tt* H-NOX I5L mutant, its α/β bands decrease by 3 and 8 nm to 572 and 539 nm, respectively. The largest blue shift is observed in the α/β region for the *Tt* H-NOX I5L/P115A mutant (7 and 12 nm, respectively).

As previously shown, *Tt* H-NOX produces a stable 6-coordinate, low-spin O_2 complex upon exposure of a reduced sample to air (19). The mutants shift by 6–7 nm to shorter wavelengths in the α/β region compared to *Tt* H-NOX WT (Soret: 416 nm, α/β bands: 591 nm and 556 nm). The largest shift is observed for the *Tt* H-NOX P115A mutant with α/β bands at ~584 and ~548 nm.

In summary, the NO and O_2 complexes show consistent shifts in the α/β bands toward shorter wavelengths upon mutating Ile-5 and Pro-115 in *Tt* H-NOX, whereas the unligated and CO complexes exhibit both shorter and longer wavelength changes for the mutants. The overall changes observed in the electronic absorption spectra are relatively minor, but consistently reproducible. These observed shifts are plausibly introduced from structural rearrangements

within the heme pocket, which then change the internal electric field. However, interpreting the changes in the α/β region is more complicated due to the different factors that influence its shape and splitting pattern, including contributions from electronic and vibronic perturbations, heme-protein interactions, and vibronic coupling strength redistributions (31).

Resonance Raman spectroscopy

To better characterize the effects of mutating Ile-5 and Pro-115 on the *Tt* H-NOX heme solution structure, we performed resonance Raman measurements on the unligated and oxygenated forms (Figure 2 and Figure 3). The main heme skeletal marker bands, v_4, v_3, v_2, and v_{10}, are summarized in Table 2 and compared to other proteins (32). The π-electron density marker (v_4), assigned as the pyrrole breathing mode, varies between 1350–1380 cm^{-1} depending on the oxidation state of the heme. The spin and coordination state markers, v_3, v_2, and v_{10}, correspond to C_α-C_m and C_β-C_β stretching vibrations in the macrocycle (21,23). Together, these skeletal markers in the 1350–1650 cm^{-1} region can be used to detect different conformations as a result of their sensitivity to the porphyrin core size and π-conjugation. In addition, the Fe-His stretching vibration at ~220 cm^{-1} is a sensitive probe of the bound histidine, providing unique structural details about the heme environment in the proximal pocket (33).

The resonance Raman spectra of the fully reduced, 5-coordinate *Tt* H-NOX WT and P115A mutant were obtained to investigate the effect of the proximal Pro-115 mutation on the Fe-His bond strength. The vibrational frequencies and intensities are similar, with the exception of the 6 cm^{-1} increase for the Fe-His stretch to 223 cm^{-1} for P115A and a ~5 cm^{-1} increase in bandwidth. In the high frequency region, the skeletal markers at 1353, 1469, 1565, and 1600 cm^{-1} correspond to typical v_4, v_3, v_2, and v_{10} values for 5-coordinate, histidyl-ligated, high-spin heme proteins (32,34,35). The striking spectral similarity between the *Tt* H-NOX WT spectrum and that of P115A in Figure 2 suggests that the heme conformation is minimally perturbed by this mutation, although the Fe-His bond length may have decreased slightly.

The resonance Raman spectra of the O_2 complexes are compared in Figure 3 and the vibrational frequencies are also summarized in Table 2. The $^{18}O_2$-isotopically substituted RR spectra are indicated with dotted lines and overlaid upon the natural abundance O_2 complex spectra in the lower frequency region to assign the Fe-O_2 stretch (Figure 3, traces a-f). Based on the simple harmonic oscillator model, a downshift of 21 cm^{-1} is predicted for v(Fe-O_2) upon $^{16}O_2$ → $^{18}O_2$ substitution. As previously shown (19), *Tt* H-NOX WT displays a v(Fe-O_2) band at 567 cm^{-1} which shifts to 540 cm^{-1} for the $^{18}O_2$ complex. Mutating Pro-115 and Ile-5 causes small downshifts of 2 to 5 cm^{-1} relative to *Tt* H-NOX WT. The *Tt* H-NOX P115A mutant exhibits an isotope-sensitive band at 565 cm^{-1} which decreases by 20 cm^{-1} for the $^{18}O_2$ complex, corresponding very well with the expected downshift. Similarly, v(Fe-O_2) for the *Tt* H-NOX I5L/P115A double mutant is observed at 562 cm^{-1} and it decreases by 25 cm^{-1} upon $^{18}O_2$ substitution. A cumulative downshift is observed for v(Fe-O_2) upon addition of the second mutation. This further decrease in frequency for the double mutant can plausibly be explained by a greater disruption of critical nonbonded contacts within the heme pocket that work to stabilize the O_2 complex.

In the high frequency region of the O_2 complexes (Figure 3, traces g-l), the skeletal markers at 1375, 1499, 1579, and 1624 cm^{-1} for *Tt* H-NOX WT are indicative of a 6-coordinate, histidyl-ligated, low-spin O_2 complex (34,36). Compared to *Tt* H-NOX WT, the three mutants show upshifts of 1–7 cm^{-1} for the skeletal markers (Table 2). Similar to the globins, the *Tt* H-NOX P115A mutant completely lacks a shoulder band at 1189 cm^{-1}, whereas WT and the other mutants exhibit two overlapping bands at 1176 cm^{-1} and 1189 cm^{-1}. In *Tt* H-NOX, v_3 remains constant at 1499 cm^{-1} for WT and the I5L mutant, but shifts to 1503 and 1502 cm^{-1} for the P115A and I5L/P115A mutants, respectively. The 1556 cm^{-1} peak is most pronounced

in *Tt* H-NOX WT and P115A, but appears more as a broad shoulder in the I5L and I5L/P115A mutants. Furthermore, ν_2 (1579 cm^{-1}) and ν_{19} (1594 cm^{-1}) in *Tt* H-NOX WT upshift by 2–3 cm^{-1} and 5 cm^{-1}, respectively, upon mutating Ile-5 and Pro-115; these two bands correspond to C_β-C_β and C_α-C_m stretching vibrations. The breadth and slight asymmetry of ν_{10} (C_α-C_m stretch) in *Tt* H-NOX WT is likely due to overlap with the C=C stretching mode at 1619 cm^{-1} (assignment based on polarization and Q-band RR). Compared to *Tt* H-NOX WT (1624 cm^{-1}), ν_{10} upshifts to 1631, 1627, and 1630 cm^{-1} for the *Tt* H-NOX P115A, I5L, and I5L/P115A mutants. These observed vibrational shifts in the high frequency region is reflective of the approximate shift pattern expected for changes in heme ruffling ($\nu_{10} > \nu_2 > \nu_3 > \nu_4$). However, closer inspection of the high frequency region reveals shoulders for ν_{10} in *Tt* H-NOX P115A and I5L/P115A that correspond to the ν_{10} vibrational frequency for WT at 1624 cm^{-1}. This band broadens and exhibits decreased intensity in the three mutants; the change is most striking in *Tt* H-NOX P115A, which has been shown by crystallography to sample a range of heme conformations (20). This observed crystallographic heterogeneity in the heme conformation for *Tt* H-NOX P115A is comparable to the broadened ν_{10} in the complementary RR spectra.

Below 1000 cm^{-1}, several vibrational modes in the *Tt* H-NOX O_2 complex spectra display reduced RR intensity upon mutation of Ile-5 and Pro-115. Heme out-of-plane modes (defined as γ to distinguish them from stretching modes, ν) involving bending, tilting, folding, and wagging motions occur in these lower frequency regions (21). The reduced RR intensities mainly occur in the 675–850 cm^{-1} and 900–1050 cm^{-1} regions as indicated by the vertical dashed lines in Figure 3 (traces a-d). Specifically, *Tt* H-NOX WT (trace a) exhibits peaks at 694 (γ_{15}, sym. pyr fold), 704 (γ_{11}, asym. pyr fold), 737 (γ_5, sym. pyr fold), 944 [$\delta(C_m$-H)], and 997 cm^{-1} [$\delta(C_m$-H)] which decrease in relative RR intensity after mutating Ile-5 and Pro-115; the most striking change occurs at 694 cm^{-1}. This band may be attributed to an in-plane pyrrole ring folding deformation mode (10). Subtle changes are also observed in the overlapping *Tt* H-NOX WT bands in the 500–640 cm^{-1} region, which are likely due to pyrrole swivels and folding vibrations (1,5,21). Of particular note are the weak bands at 526 (ν_{49}), 589 (ν_{48}), 605 (sym. pyr fold) and 636 cm^{-1} (γ_{20}, asym. pyr fold) in *Tt* H-NOX WT that vanish in the *Tt* H-NOX P115A mutant. These peaks are still present in the *Tt* H-NOX I5L and I5L/P115A mutants, albeit slightly broader and lower in intensity than WT. The 271 cm^{-1} band in *Tt* H-NOX WT also broadens and downshifts by 9 cm^{-1} in the P115A mutant to 262 cm^{-1}; this peak may correspond to either ν_{52} (porph-substituent bending) or a pyrrole tilting motion (γ_{16}) within the heme (2,37).

Spectral decomposition

The RR intensity decreased for several low frequency modes in the O_2 complexes for the *Tt* H-NOX mutants (Figure 3), but remained constant in the unligated (Figure 2; supplementary material, Figure 1S) and CO complexes (supplementary material, Figure 3S). These bands may show changes in intensity due to the inactivation of Raman modes upon heme relaxation. To quantify these spectral changes, the RR spectra were normalized and fit to Lorentzian peaks with fixed widths. The integrated peak areas are shown in Figure 4 to compare the RR intensity changes across *Tt* H-NOX WT and mutants. Intensity decreases of ~30–70% are observed upon mutating Ile-5 and Pro-115. In addition, the 704 cm^{-1} peak (γ_{11}, asym. pyrrole folding) in *Tt* H-NOX WT broadens and develops a small shoulder at 709–712 cm^{-1}, shifting toward the higher frequency band and decreasing in RR intensity in the mutants. Two different trends in the RR intensities were noted (the bars in Figure 4 are shaded differently to denote the two trends): one shows the intensity steadily decreasing across all mutants, whereas the other trend displays a zigzag pattern due to the minimal to moderate intensity change observed in *Tt* H-NOX I5L compared to the other two mutants.

Normal coordinate structural decomposition

Table 3 quantifies the calculated heme out-of-plane (oop) distortions for the O_2 complexes of *Tt* H-NOX and other proteins from our NSD analysis (7). The generated output gives the amount of displacement along the normal coordinates for the six deformation types (*e.g.* ruffling, saddling) that properly simulate the observed distortions in the *Tt* H-NOX heme coordinates. NSD results obtained from other heme proteins are included for comparison. The total out-of-plane displacement (Δ_{oop}) and the amount of specific deformation types are reported according to the complete and minimal basis sets, respectively. The complete basis set includes all normal modes of the 24 atom D_{4h}-symmetric porphyrin macrocycle ($C_{20}N_4$) to fully describe the observed heme nonplanarity. The minimal basis set only includes the lowest frequency normal coordinates of each symmetry type (6 in-plane and 6 out-of-plane) since these are expected to have the lowest distortion energies and should be predominant in the heme deformations (4,13).

As shown in Table 3, the largest displacements observed in the *Tt* H-NOX WT monoclinic (PDB 1U55) and orthorhombic (PDB 1U4H) crystal structures are from the B_{2u} (saddling) and B_{1u} (ruffling) deformations. The total rms out-of-plane displacement (Δ_{oop}) is ~1.6 Å for three different *Tt* H-NOX WT structures, but is reduced to ~1.1 Å in the monoclinic heme B structure. Pellicena *et al.* associate this heme relaxation with a ~11° rotation of the protein's distal portion with respect to the proximal side and a reorientation of the distal Ile-5 residue (14). With the exception of the monoclinic heme B structure, the other three *Tt* H-NOX WT hemes maintain ~1.0–1.2 Å displacements in B_{1u} and B_{2u} deformations.

Compared to *Tt* H-NOX WT (Δ_{oop} ~1.6 Å), the *Tt* H-NOX I5L mutant showed a decrease of ~0.2–0.3 Å in overall out-of-plane displacement. The B_{1u} deformation is more relaxed than B_{2u} in *Tt* H-NOX I5L, but a small increase occurs in the $E_{g(x,y)}$ (waving) displacement. In addition, the B_{1u} directionality changes sign between the two *Tt* H-NOX I5L heme molecules. This also occurs for several deformations in the truncated and human hemoglobins (PDB 1IDR and 2DN1, respectively), and may result from differences in the crystal packing interactions and orientation of residues close to the heme.

The crystal structure of *Tt* H-NOX P115A contained four different hemes, producing a broader range of NSD displacements compared to the other proteins (PDB 3EEE). The most relaxed structure (heme C) exhibited out-of-plane distortion values (B_{2u}, −0.04 Å; B_{1u}, −0.49 Å; Δ_{oop}, 0.54 Å) comparable to those obtained for the crystal structures of *Bj* FixL (26) and the globins (27–29). The Δ_{oop} for these proteins ranged from 0.36 to 0.60 Å in contrast to *Tt* H-NOX WT (~1.6 Å). The total out-of-plane displacement for the least relaxed *Tt* H-NOX P115A structure (heme A) is 0.90 Å, which is close to the 1.11 Å Δ_{oop} observed for the monoclinic *Tt* H-NOX WT heme B structure.

The *Tt* H-NOX double mutant significantly relaxed the ruffling distortion with a B_{1u} displacement of ~0.05–0.2 Å. Comparable to *Sw* Mb, these magnitudes are the lowest of the three *Tt* H-NOX mutants. In contrast, the B_{2u} displacement (heme A, −0.53 Å; heme B, −0.63 Å) is greater than the < 0.1 Å observed in hemes C and D of the P115A mutant. Another unique feature exhibited by the double mutant is the ~0.3–0.5 Å $E_{g(y)}$ contribution, which is similar to *Tt* H-NOX I5L heme A (0.4 Å). Interestingly, the Δ_{oop} for *Tt* H-NOX I5L/P115A (heme A, 0.85 Å; heme B, 0.74 Å) falls within the ~0.5 – 0.9 Å range obtained for the four *Tt* H-NOX P115A heme molecules, suggesting that the Ile-5 mutation contributes minimally to heme relaxation.

DISCUSSION

We now provide a detailed interpretation of the spectral changes exhibited by RR leading to the current model for heme distortion in *Tt* H-NOX. Specifically, the reduction in relative RR intensity for the low frequency modes, and the observed frequency shifts and peak broadening in the heme skeletal markers of *Tt* H-NOX P115A and I5L mutants provide evidence for a more relaxed chromophore within the solution form of the mutated protein. These changes are related to the heme structure and how its altered conformation, in comparison to *Tt* H-NOX WT, may result from heme cavity rearrangements. By comparing the spectroscopic data with the available crystallographic results, detailed information on the heme structure and insight into the possible role of these conserved residues are revealed.

RR intensity changes in Tt H-NOX O$_2$ complex spectra

Choi and Spiro identified several out-of-plane motions of iron-porphyrin complexes, including pyrrole tilts (~260 cm^{-1}), methine bridge deformations [$\gamma(C_\alpha\text{-}C_m)$, ~320 cm^{-1}], pyrrole folding modes (~425–510 cm^{-1}), and methine-hydrogen deformations [$\gamma(C_m\text{-}H)$, ~840 cm^{-1}] (10). Modes that occur below 400 cm^{-1} involve methine bridge wagging and other pyrrole deformations, and are expected to be heavily mixed (21). These out-of-plane modes are generally expected to be Franck-Condon and Jahn-Teller inactive for planar porphines of D_{4h} symmetry, but may be activated upon nonplanar heme distortion and symmetry reduction (5,10). The RR intensities of these modes are induced when their components are projected onto the in-plane electronic excitations (2,10). Hence, only the modes that occur along specific heme distortion coordinates and have the same symmetry will be activated.

Our RR spectra of *Tt* H-NOX WT exhibit several bands corresponding to out-of-plane modes associated with heme deformations in the O$_2$ complex. Specifically, the 450–600 cm^{-1} region displays many overlapped Raman features that are plausibly out-of-plane pyrrole tilts, swivels, and folding modes activated by the symmetry lowering effects of the protein environment on the chromophore. Other notable features include the moderately intense 692 cm^{-1} shoulder (γ_{15}, sym. pyrrole folding), the 704 peak with a small shoulder at 712 cm^{-1} (γ_{11}, sym. pyrrole folding), and the 737 cm^{-1} band (γ_5/ν_{16}, asym. pyrrole folding and deformation). These peaks are known to be sensitive to saddling (B_{2u}) and ruffling (B_{1u}) deformations, and are tentatively assigned by association with previous work by Spiro, Shelnutt, Schweitzer-Stenner, and others (1,2,5,10,11,21,38,39). Between 900–1000 cm^{-1}, four distinct peaks observed in the *Tt* H-NOX WT spectrum are tentatively assigned as hydrogen wagging motions (37). These RR features confirm that the striking heme deformations observed in the *Tt* H-NOX WT structure also exist in solution and are not an outcome of crystallization. Interestingly, these characteristic low frequency bands in the *Tt* H-NOX spectra are unique to the O$_2$ complex, and are not prominently featured in the other *Tt* H-NOX complexes or bacterial H-NOXs (*e.g. V. cholerae*, *L. pneumophila*, *N. punctiforme*) (19,24). In agreement with these observations, NSD analysis of the *N. sp* H-NOX domain crystal structures by Ma *et al.* indicate Δ_{oop} ~ 0.7–0.9 Å for the unligated, CO, and NO complexes; these values are lower than those observed for the *Tt* H-NOX O$_2$ structures by Pellicena *et al.* (Δ_{oop} ~ 1.1–1.6 Å) (14,16).

Mutation of the Ile-5 and Pro-115 residues in *Tt* H-NOX caused decreases in the relative RR intensities for several out-of-plane modes in the O$_2$ complex, but did not appreciably alter any mode intensities in the unligated spectra. These observations indicate a distinct difference in how the mutations affect the heme conformation for the O$_2$ and unligated species; although significant structural changes occur in the O$_2$ complex, the great similarity in RR intensity for the unligated spectra strongly suggests minimal changes in the heme structure. The most important point about the loss of RR intensity is that it clearly demonstrates a relaxation of the heme upon mutating these residues. The replacement of Pro-115 in *Tt* H-NOX with an alanine relieves the original proximal strain on pyrrole group D by freeing up space around the random

coil linking α-helix F and β-strand 1. This structural reorganization is consistent with the loss of RR intensity at 508 (γ_{12}), 526 (ν_{49}), 588 (ν_{48}), and the 692–737 cm^{-1} region (γ_{15}, γ_{11}, γ_5), where pyrrole swivels and folding modes that correspond to the B$_{1u}$, B$_{2u}$, and E$_g$ symmetry are expected to occur (1,2,5,38,39). A similar effect, albeit to a lesser degree, can explain the changes in the *Tt* H-NOX I5L spectra via its distal strain over pyrrole A and influence on reorienting nearby residue contacts with the propionate groups (*e.g.* Asp-45).

Although the three *Tt* H-NOX mutants showed comparable decreases in relative RR intensity for some of the low frequency bands, the P115A mutant displayed several distinct features. These included the following observations: (i) the apparent absence of the 1189 cm^{-1} peak corresponding to the C$_\beta$-substituent and C$_\alpha$-N antisymmetric stretching modes, which is also exhibited in the globins spectra, (ii) the retention of the hydrogen wagging modes (850–1050 cm^{-1}) in *Tt* H-NOX I5L compared to the P115A mutant, and (iii) the greater similarity in peakwidth and frequency between the *Tt* H-NOX I5L and WT spectra in comparison to P115A. In addition, the locations where RR intensity is lost after mutating the heme pocket residues correspond well to the less congested regions in the globin spectra, supporting our tentative assignment of these peaks to heme out-of-plane modes. These characteristics together support a more dominant effect of Pro-115 on the *Tt* H-NOX heme structure than Ile-5.

Our spectral observations also fit well with the structural data via the NSD analysis, which indicates that the lowest Δ_{oop} occurs in *Tt* H-NOX P115A (heme C; $\Delta_{oop} \sim 0.5$ Å) rather than the double mutant. The Δ_{oop} range of ~0.5–0.9 Å for all four molecules in the unit cell and the differing effects on the B$_{2u}$ and B$_{1u}$ deformations further support the heme flexibility that we observed by RR in the *Tt* H-NOX P115A mutant. According to the NSD analysis, the *Tt* H-NOX I5L mutation affected the B$_{2u}$ displacement less than B$_{1u}$; this effect may explain the two trends shown in the spectral decomposition in that some modes may be more sensitive and specific to certain heme deformations. In addition, the normal mode displacements for *Tt* H-NOX I5L displayed modest decreases compared to *Tt* H-NOX P115A, which agrees well with our conclusions from the RR spectra. Finally, the cumulative decrease in relative RR intensity exhibited by the double mutant was close to those observed for the single *Tt* H-NOX P115A mutant, further suggesting that the dominant perturbation of the pocket originates from the Pro-115 mutation. This reduction of the B$_{2u}$ and B$_{1u}$ deformations can be rationalized based on the nonbonded contacts between Pro-115 and pyrrole group C of the heme (Figure 1 and Figure 5). The proline ring clearly pushes up into the heme and forces the chromophore into a nonplanar conformation. Upon substitution with alanine, the ring is substituted by a more freely rotating methyl group, which allows the heme conformation to relax (Figure 5). In contrast to Pro-115, Ile-5 makes a less intrusive distal contact with the heme pyrrole group B in *Tt* H-NOX; thus, mutating this residue has a smaller effect on the heme conformation.

Frequency shifts and peak broadening

In contrast to the pronounced changes observed in the O$_2$ complex spectra, the great similarity in vibrational frequency and intensity between the RR spectra for the *Tt* H-NOX WT and P115A unligated species demonstrates the minimal impact of this mutation on the heme. The increased Fe-His stretching frequency for *Tt* H-NOX P115A suggests a strengthening of the Fe-His bond. In contrast, crystallographic results indicate that the bond lengths for the two proteins are within error. This discrepancy is not surprising since in resonance Raman spectroscopy, a vibrational frequency shift of 5–6 cm^{-1} in the most sensitive bands corresponds to bond length changes of as small as 0.01 Å (21,33). Such a change would be below the range detectable by crystallography. Olea *et al.* do note, however, that the Fe-His bond tilting angle shifts from 78° in *Tt* H-NOX WT (heme A, monoclinic) to 87° in P115A (heme C, monoclinic), resulting in a more perpendicular orientation of His-102 with respect to the heme, and plausibly enables a better bond overlap between Fe and His-102 (20). Furthermore, the slight broadening of the

peak by ~5 cm^{-1} suggests some heterogeneity in the proximal pocket, and supports our assertion that the *Tt* H-NOX P115A mutation introduces structural disorder and flexibility to the protein pocket. This heterogeneity in the RR spectra fits well with the 80–87° Fe-His tilt angle range reported for the four *Tt* H-NOX P115A heme molecules (20).

Kinetic studies by Olea *et al.* on *Tt* H-NOX have shown that the O_2 dissociation rates decrease by an order of magnitude between WT (1.22 ± 0.09 s^{-1}) and the P115A mutant (0.22 ± 0.01 s^{-1}), but that the O_2 association rates are similar (13.6 ± 1.0 $\mu M^{-1}s^{-1}$ and 10.4 ± 1.1 $\mu M^{-1}s^{-1}$, respectively) (20). Our RR results exhibit a small cumulative downshift in the ν(Fe-O_2) frequency with the three *Tt* H-NOX mutants from 567–570 cm^{-1} (WT) to 562 cm^{-1} (I5L/P115A mutant). In addition, the P115A mutant exhibits a 6 cm^{-1} downshift to 265 cm^{-1} from WT (271 cm^{-1}); this band may be a combination of in-plane Fe-N_{pyr} stretching, pyrrole tilting, and pyrrole-substituent bending motions (ν_{52}). Irwin *et al.* previously proposed that a stronger ligand field could arise from a constrained heme along the equatorial porphyrin plane (40). Since heme ruffling is thought to result in a shortening of the equatorial Fe-N_{pyr} bonds, this may partly explain the different frequencies observed between *Tt* H-NOX WT and the mutants for ν(Fe-O_2) and ν(Fe-N_{pyr}), although other factors within the protein pocket (*e.g.* hydrogen-bonding residues, tension on the trans-Fe-imidazole bond, and steric bulk) also clearly influence the stability of the O_2 complex. In particular, the ruffling deformation/Fe-N_{pyr} bond distance dependence is consistent with our observed ν(Fe-N_{pyr}) downshift for the *Tt* H-NOX P115A mutant, which also exhibits a relaxation of the ruffling deformation. In contrast, the crystal structures indicate that the Fe-N_{pyr} distances are ~2.0 Å for both *Tt* H-NOX WT and P115A with only a negligible decrease for the WT Fe-N_{pyr} distance. However, based on Badger's Rule (41,42), the inverse force constant/bond length relationship shows that the vibrational frequency is more sensitive to small changes (~0.01 Å) in internuclear distance. Thus, the discrepancy between the RR spectra and crystal structure can be readily explained.

Structural heterogeneity in a sample can be revealed by the broadness and asymmetry of structure sensitive lines, such as ν_2 (C_β-C_β stretch) and ν_{10} (C_α-C_m stretch) (11). Our RR results exhibit several regions in which the peaks broaden upon mutating Ile-5 and Pro-115 in *Tt* H-NOX. The clearest example of this is ν_{10} in the P115A mutant; in comparison to the WT spectra, this band decreases in intensity and broadens to display a prominent shoulder band at 1631 cm^{-1}. Broad features are also observed for the *Tt* H-NOX Ile-5 and double mutants in the 1550–1600 cm^{-1} range; the modes in this region correspond to the C_α-C_m, C_β-C_β, and peripheral vinyl modes. The broadening of these distinct peaks into merged bands suggests conformational flexibility in these regions, and may result from the ability of the Leu-5 side chain to rapidly flip directions within the pocket. These fluctuations likely disrupt the contacts between the protein's YSR motif and the nearby propionate groups. Furthermore, the fact that ν_2 and ν_{10} upshift in frequency for all three *Tt* H-NOX mutants supports the possibility of a better π-π overlap in the C=C, C_β-C_β, and C_α-C_m bonds within the porphyrin macrocycle as a result of heme relaxation.

Some peak broadening and shoulder band formation also occur below 450 cm^{-1}, where pyrrole deformations are expected to occur. The 423 cm^{-1} peak [δ(C_β-vinyl)] in *Tt* H-NOX WT not only downshifts to 417 cm^{-1} (P115A), but also broadens with a weak shoulder band and slight decrease in RR intensity. Several other bands in this region exhibit similar changes. These observations further support the possibility that the *Tt* H-NOX protein pocket no longer firmly holds the heme in a particular conformation.

Possible role for conserved residues and heme deformation in Tt H-NOX

The heme deformation in the H-NOX family plausibly plays a role in signal transduction from the chromophore to the protein upon ligand binding; alteration of the heme conformation may induce protein conformational changes, which then regulate the linked signaling protein (e.g.

histidine kinases, diguanylate cyclases, and MCP domains). Based on our data, we conclude that the single P115A mutation is sufficient to open the *Tt* H-NOX distal pocket and introduce flexibility to the heme structure, enabling the chromophore to relax and sample other conformations. The possibility of the H-NOX domain alternating between closed and open conformations is reasonable based on previously observed varying rotational angles in the H-NOX distal and proximal subdomains (14,16,20). Similar to the protein conformation changes observed by Pellicena *et al.* (14) in the *Tt* H-NOX WT monoclinic structure (heme B), a plausible explanation for P115A's spectral changes is that the distal pocket has more rotational motion, and may sample an open heme pocket more frequently due to the increased flexibility granted by replacing the rigidly kinked proline ring with the more freely rotating alanine methyl group. Thus, the highly conserved Pro-115 and neighboring residues can serve as a hinge point between the N- and C-terminal subdomains, which are necessary for maintaining an enclosed environment, retaining important heme-protein interactions, and conserving specific biochemical properties within the H-NOX protein pocket. A clear example of this is the dramatic changes observed in the reduction potential and O_2 affinity upon decreasing the amount of heme distortion present in *Tt* H-NOX (20). The *Tt* H-NOX I5L mutation may also contribute toward opening the pocket, although to a lesser extent based on the more modest spectral changes and shifts exhibited by this single mutant in comparison to those observed by mutating Pro-115. This result is not surprising since the substitution of Ile with Leu is relatively conservative in comparison to the replacement of the proline with alanine. However, this Leu-5 side chain can also plausibly flip inward toward the distal pocket or away from it; thus, the heme may interact differently with the conserved YSR motif, depending on whether or not the chromophore is pinned down along pyrrole group A by the aliphatic chain.

In summary, we provide spectral evidence of heme relaxation in the O_2-bound form of *Tt* H-NOX upon mutating the Ile-5 and Pro-115 residues. Our resonance Raman results exhibit the most significant changes in the *Tt* H-NOX P115A mutant, in contrast to the I5L mutation, which bears spectral features more similar to *Tt* H-NOX WT. Furthermore, the double mutant appears to behave more like an admixture of P115A with I5L, rather than a synergistic combination of the two mutations. In addition, we observe some broad shoulder features in the high frequency region that suggest the presence of other heme conformations in the three *Tt* H-NOX mutants. Of the different heme complex forms that we have studied with resonance Raman, the most striking changes occur in the O_2-bound spectra; we see very little change in the unligated and CO complexes. These results provide a clear insight into the actual heme conformation of *Tt* H-NOX P115A in solution; indicating that although it is heterogeneous, the predominant form is significantly relaxed based on both changes in vibrational frequencies and RR out-of-plane mode intensities.

Supplementary Material

Refer to Web version on PubMed Central for supplementary material.

Abbreviations

H-NOX, Heme-Nitric Oxide and/or Oxygen binding domain; RR, resonance Raman; *Tt*, *Thermoanaerobacter tengcongensis*; TEA, triethanolamine; DFT, density functional theory; QM/MM, quantum mechanics/molecular mechanics; NSD, normal coordinate structural decomposition; Δ_{oop}, total out-of-plane displacement.

ACKNOWLEDGMENTS

REFERENCES

1. Blackwood ME, Rush TS, Medlock A, Dailey HA, Spiro TG. Resonance Raman spectra of ferrochelatase reveal porphyrin distortion upon metal binding. J. Am. Chem. Soc 1997;119:12170–12174.

2. Jarzecki AA, Spiro TG. Porphyrin distortion from resonance Raman intensities of out-of-plane modes: Computation and modeling of N-methylmesoporphlyrin, a ferrochelatase transition state analog. J. Phys. Chem. A 2005;109:421–430. [PubMed: 16833362]

3. Sparks LD, Anderson KK, Medforth CJ, Smith KM, Shelnutt JA. Correlations between Raman Frequencies and Structure for Planar and Nonplanar Metalloporphyrins. Inorg. Chem 1994;33:2297–2302.

4. Jentzen W, Ma JG, Shelnutt JA. Conservation of the conformation of the porphyrin macrocycle in hemoproteins. Biophys. J 1998;74:753–763. [PubMed: 9533688]

5. Huang Q, Medforth CJ, Schweitzer-Stenner R. Nonplanar heme deformations and excited state displacements in nickel porphyrins detected by Raman spectroscopy at Soret excitation. J. Phys. Chem. A 2005;109:10493–10502. [PubMed: 16834304]

6. Sigfridsson E, Ryde U. The importance of porphyrin distortions for the ferrochelatase reaction. J. Biol. Inorg. Chem 2003;8:273–282. [PubMed: 12589563]

7. Shelnutt JA, Song XZ, Ma JG, Jia SL, Jentzen W, Medforth CJ. Nonplanar porphyrins and their significance in proteins. Chem. Soc. Rev 1998;27:31–41.

8. Kozlowski PM, Rush TS, Jarzecki AA, Zgierski MZ, Chase B, Piffat C, Ye BH, Li XY, Pulay P, Spiro TG. DFT-SQM force field for nickel porphine: Intrinsic ruffling. J. Phys. Chem. A 1999;103:1357–1366.

9. Xu CL, Ibrahim M, Spiro TG. DFT analysis of axial and equatorial effects on Heme-CO vibrational modes: Applications to CooA and H-NOX heme sensor proteins. Biochemistry 2008;47:2379–2387. [PubMed: 18217776]

10. Choi SH, Spiro TG. Out-of-Plane Deformation Modes in the Resonance Raman Spectra of Metalloporphyrins and Heme Proteins. J. Am. Chem. Soc 1983;105:3683–3692.

11. Jentzen W, Simpson MC, Hobbs JD, Song X, Ema T, Nelson NY, Medforth CJ, Smith KM, Veyrat M, Mazzanti M, Ramasseul R, Marchon JC, Takeuchi T, Goddard WA, Shelnutt JA. Ruffling in a Series of Nickel(II) Meso-Tetrasubstituted Porphyrins as a Model for the Conserved Ruffling of the Heme of Cytochromes-c. J. Am. Chem. Soc 1995;117:11085–11097.

12. Czernuszewicz RS, Li XY, Spiro TG. Nickel Octaethylporphyrin Ruffling Dynamics from Resonance Raman Spectroscopy. J. Am. Chem. Soc 1989;111:7024–7031.

13. Jentzen W, Song XZ, Shelnutt JA. Structural characterization of synthetic and protein-bound porphyrins in terms of the lowest-frequency normal coordinates of the macrocycle. J. Phys. Chem. B 1997;101:1684–1699.

14. Pellicena P, Karow DS, Boon EM, Marletta MA, Kuriyan J. Crystal structure of an oxygen-binding heme domain related to soluble guanylate cyclases. Proc. Natl. Acad. Sci. U.S.A 2004;101:12854–12859. [PubMed: 15326296]

15. Nioche P, Berka V, Vipond J, Minton N, Tsai AL, Raman CS. Femtomolar sensitivity of a NO sensor from *Clostridium botulinum*. Science 2004;306:1550–1553. [PubMed: 15472039]

16. Ma XL, Sayed N, Beuve A, van den Akker F. NO and CO differentially activate soluble guanylyl cyclase via a heme pivot-bend mechanism. EMBO J 2007;26:578–588. [PubMed: 17215864]

17. Boon EM, Marletta MA. Ligand specificity of H-NOX domains: from sGC to bacterial NO sensors. J. Inorg. Biochem 2005;99:892–902. [PubMed: 15811506]

18. Gilles-Gonzalez MA, Gonzalez G. Heme-based sensors: defining characteristics, recent developments, and regulatory hypotheses. J. Inorg. Biochem 2005;99:1–22. [PubMed: 15598487]

19. Karow DS, Pan D, Tran R, Pellicena P, Presley A, Mathies RA, Marletta MA. Spectroscopic characterization of the soluble guanylate cyclase-like heme domains from *Vibrio cholerae* and *Thermoanaerobacter tengcongensis*. Biochemistry 2004;43:10203–10211. [PubMed: 15287748]

20. Olea C, Boon EM, Pellicena P, Kuriyan J, Marletta MA. Probing the Function of Heme Distortion in the H-NOX Family. ACS Chem. Biol 2008;3:703–710. [PubMed: 19032091]

21. Spiro, TG.; Li, XY. Resonance Raman Spectroscopy of Metalloporphyrins. In: Spiro, TG., editor. Biological Applications of Raman Spectroscopy: Resonance Raman spectra of heme and metalloproteins. New York: John Wiley & Sons; 1988. p. 1-37.

22. Myers, AB.; Mathies, RA. "Resonance Raman Intensities: A Probe of Excited State Structure and Dynamics". In: Spiro, TG., editor. Biological Applications of Raman Spectroscopy: Resonance Raman Spectra of Polyenes and Aromatics. New York: John Wiley & Sons; 1988. p. 1-58.

23. Spiro TG, Stong JD, Stein P. Porphyrin Core Expansion and Doming in Heme Proteins - New Evidence from Resonance Raman Spectra of 6-Coordinate High-Spin Iron(III) Hemes. J. Am. Chem. Soc 1979;101:2648–2655.

24. Boon EM, Davis JH, Tran R, Karow DS, Huang SH, Pan D, Miazgowicz MM, Mathies RA, Marletta MA. Nitric oxide binding to prokaryotic homologs of the soluble guanylate cyclase β1 H-NOX domain. J. Biol. Chem 2006;281:21892–21902. [PubMed: 16728401]

25. Mathies R, Yu NT. Raman Spectroscopy with Intensified Vidicon Detectors -Study of Intact Bovine Lens Proteins. J. Raman Spectrosc 1978;7:349–352.

26. Gong W, Hao B, Chan MK. New mechanistic insights from structural studies of the oxygen-sensing domain of *Bradyrhizobium japonicum* FixL. Biochemistry 2000;39:3955–3962. [PubMed: 10747783]

27. Milani M, Pesce A, Ouellet Y, Ascenzi P, Guertin M, Bolognesi M. Mycobacterium tuberculosis hemoglobin N displays a protein tunnel suited for O_2 diffusion to the heme. EMBO J 2001;20:3902–3909. [PubMed: 11483493]

28. Vojtechovsky J, Chu K, Berendzen J, Sweet RM, Schlichting I. Crystal structures of myoglobin-ligand complexes at near-atomic resolution. Biophys. J 1999;77:2153–2174. [PubMed: 10512835]

29. Yang J, Kloek AP, Goldberg DE, Mathews FS. The structure of Ascaris hemoglobin domain I at 2.2 A resolution: molecular features of oxygen avidity. Proc. Natl. Acad. Sci. U.S.A 1995;92:4224–4228. [PubMed: 7753786]

30. Antonini, E.; Brunori, M. Hemoglobin and myoglobin in their reactions with ligands. Vol. Vol. 21. Amsterdam: North-Holland Publishing Company; 1971.

31. Levantino M, Huang Q, Cupane A, Laberge M, Hagarman A, Schweitzer-Stenner R. The importance of vibronic perturbations in ferrocytochrome c spectra: A reevnaluation of spectral properties based on low-temperature optical absorption, resonance Raman, and molecular-dynamics simulations. J. Chem. Phys 2005;123

32. Tomita T, Gonzalez G, Chang AL, Ikeda-Saito M, Gilles-Gonzalez MA. A comparative resonance Raman analysis of heme-binding PAS domains: heme iron coordination structures of the *Bj*FixL, *Ax*PDEA1, *Ec*Dos, and *Mt*Dos proteins. Biochemistry 2002;41:4819–4826. [PubMed: 11939776]

33. Kitagawa, T. The Heme Protein Structure and the Iron-Histidine Stretching Mode. In: Spiro, TG., editor. Biological Applications of Raman Spectroscopy: Resonance Raman Spectra of Heme and Metalloproteins. New York: John Wiley & Sons; 1988. p. 97-131.

34. Tamura K, Nakamura H, Tanaka Y, Oue S, Tsukamoto K, Nomura M, Tsuchiya T, Adachi S, Takahashi S, Iizuka T, Shiro Y. Nature of endogenous ligand binding to heme iron in oxygen sensor FixL. J. Am. Chem. Soc 1996;118:9434–9435.

35. Choi S, Spiro TG, Langry KC, Smith KM, Budd DL, Lamar GN. Structural Correlations and Vinyl Influences in Resonance Raman Spectra of Protoheme Complexes and Proteins. J. Am. Chem. Soc 1982;104:4345–4351.

36. Takahashi S, Ishikawa K, Takeuchi N, Ikedasaito M, Yoshida T, Rousseau DL. Oxygen-Bound Heme-Heme Oxygenase Complex - Evidence for a Highly Bent Structure of the Coordinated Oxygen. J. Am. Chem. Soc 1995;117:6002–6006.

37. Hu SZ, Smith KM, Spiro TG. Assignment of protoheme Resonance Raman spectrum by heme labeling in myoglobin. J. Am. Chem. Soc 1996;118:12638–12646.

38. Rush TS, Kozlowski PM, Piffat CA, Kumble R, Zgierski MZ, Spiro TG. Computational modeling of metalloporphyrin structure and vibrational spectra: Porphyrin ruffling in NiTPP. J. Phys. Chem. B 2000;104:5020–5034.

39. Huang Q, Schweitzer-Stenner R. Non-planar heme deformations and excited state displacements in horseradish peroxidase detected by Raman spectroscopy at Soret excitation. J. Raman Spectrosc 2005;36:363–375.

40. Irwin MJ, Armstrong RS, Wright PE. Resonance Raman Studies of Soybean Leghemoglobin and Myoglobin - Origin of the Differences in O_2 Dissociation Rate Constants. FEBS Lett 1981;133:239–243.

41. Badger RM. The relation between the internuclear distances and force constants of molecules and its application to polyatomic molecules. J. Chem. Phys 1935;3:710–714.

42. Green MT. Application of Badger's rule to heme and non-heme iron-oxygen bonds: An examination of ferryl protonation states. J. Am. Chem. Soc 2006;128:1902–1906. [PubMed: 16464091]
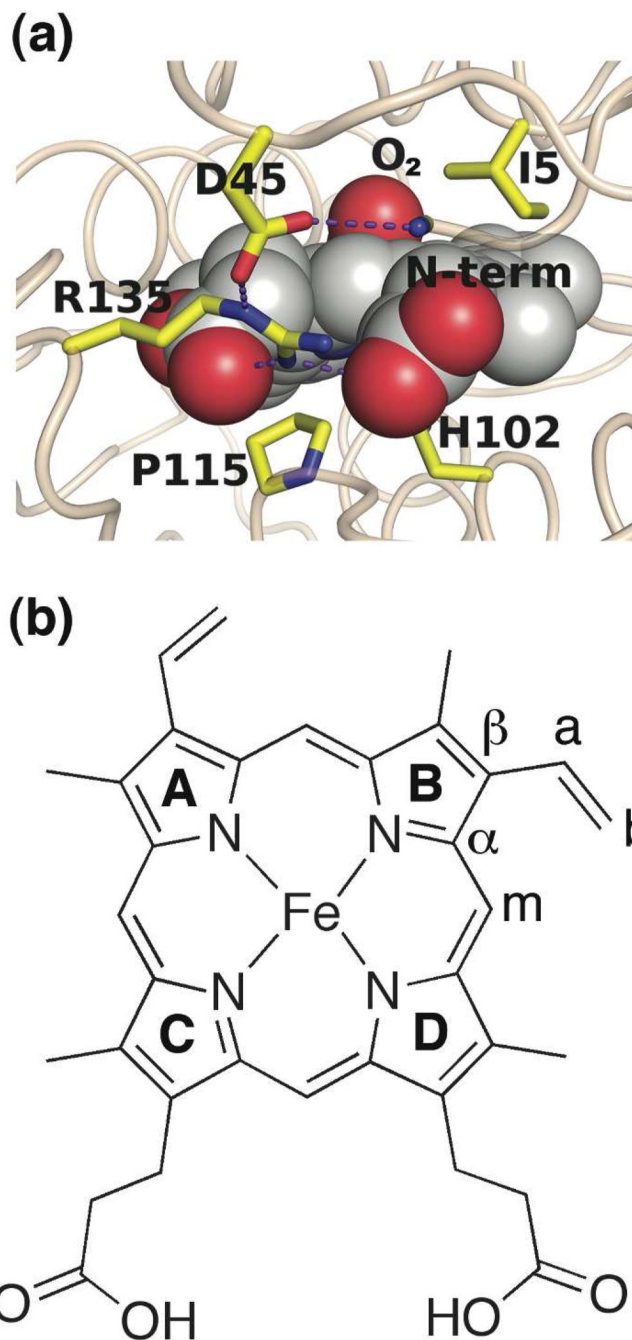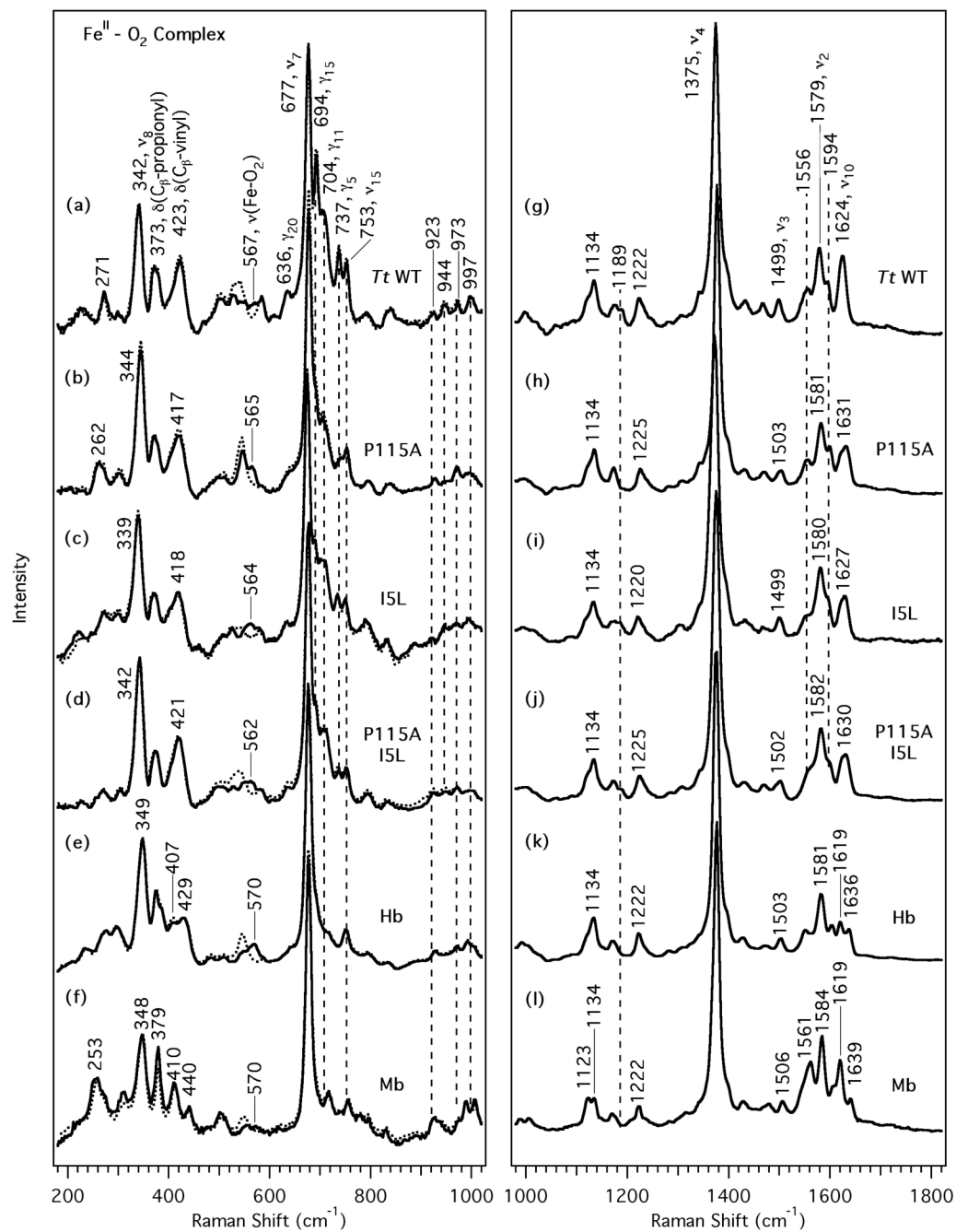
Figure 1.
(a) Structure of the heme pocket of the *Tt* H-NOX WT Fe^{II}-O_2 complex, indicating the distal Ile-5 and proximal Pro-115 thought to be responsible for the distorted heme structure (PDB 1U55). (b) Heme molecular structure and labeling scheme.
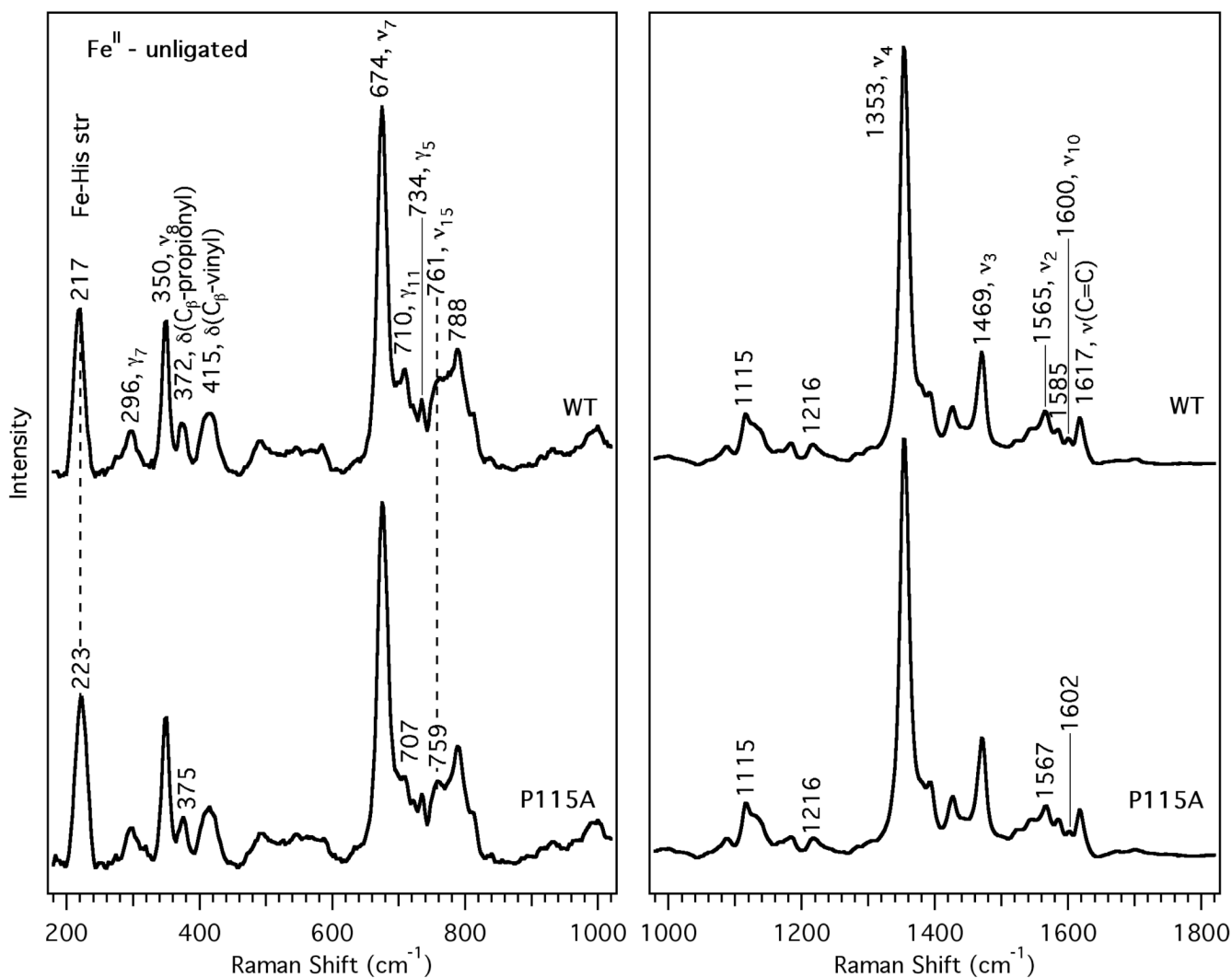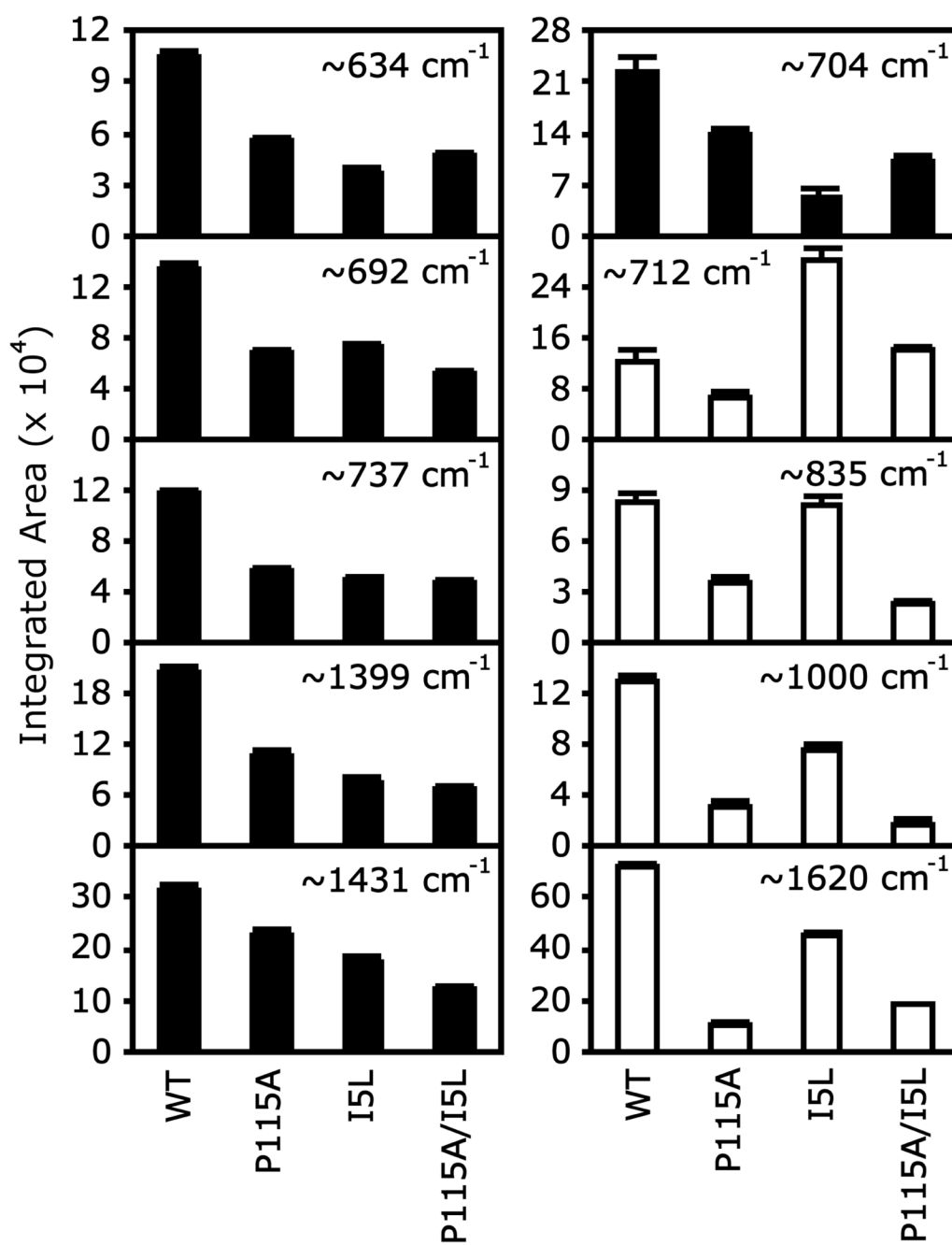
Figure 2.
Resonance Raman spectra of the Fe^{II}-unligated form of *Tt* H-NOX WT (upper trace) and P115A (lower trace). Spectral intensities in the low and high frequency regions were normalized to ν_7 and ν_4, respectively.

Figure 3.
Resonance Raman spectra of the O_2 complexes of the *Tt* H-NOX domains and globins. The left panel shows the lower frequency region for *Tt* H-NOX WT (a), P115A (b), I5L (c), P115A/ I5L (d), Hb (e), and Mb (f). $^{18}O_2$ spectra (dotted line) are overlapped over the $^{16}O_2$ spectra to indicate the frequency shifts upon isotopic substitution. The right panel shows the high frequency region (traces g-l).

Figure 4.
Integrated RR peak areas show intensity changes in *Tt* H-NOX upon mutation of Ile-5 and Pro-115. The black and white bars denote the two different trends in RR intensity changes.
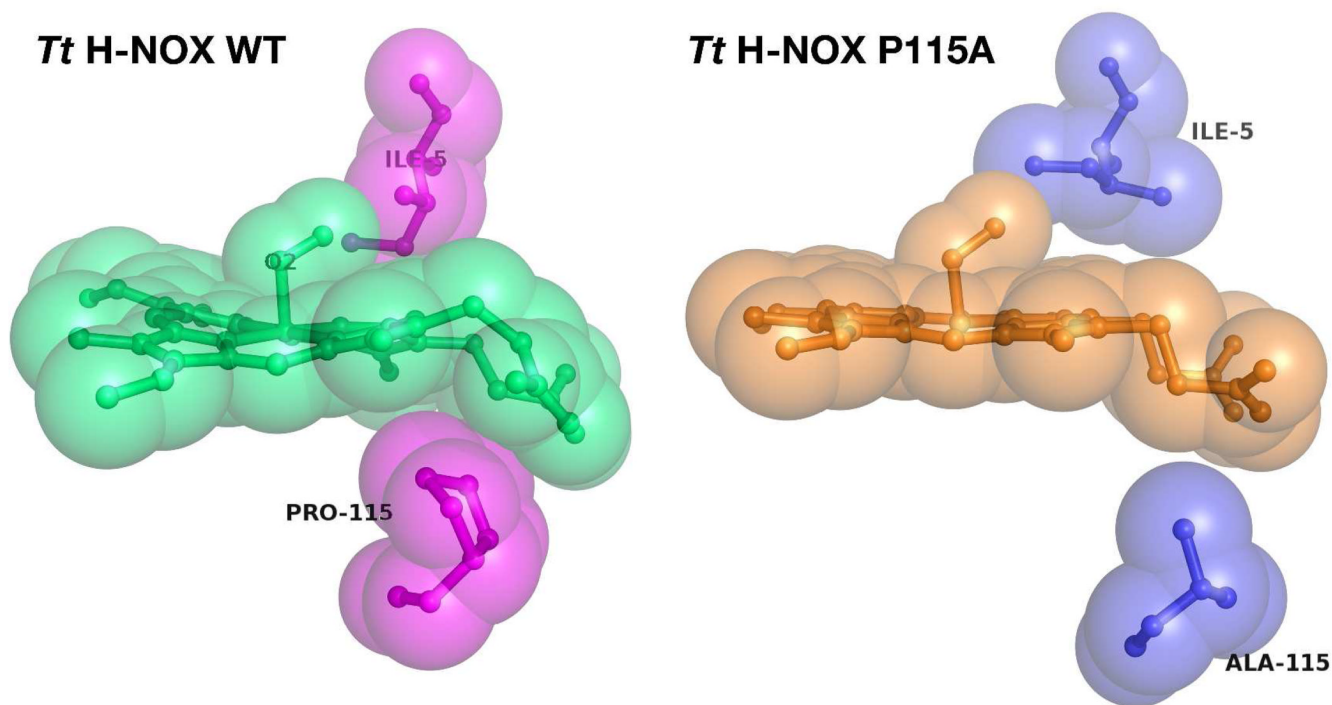
Figure 5.
Comparison of *Tt* H-NOX WT (PDB 1U55) with P115A (PDB 3EEE) showing reduction of steric nonbonded contacts between proximal Pro-115 and heme upon mutation to Ala-115.

Table 1

Electronic absorption properties for *Tt* H-NOX, Hb, and Mb in the reduced and CO, NO, and O₂-bound forms.[a]

Protein	Ligand	Soret	α/β	Ref.
Tt WT	reduced	430	563	(19)
Tt P115A		432	563	this work
Tt I5L		431	569	this work
Tt P115A/I5L		431	566	this work
Hb		430	555	(30)
Mb		434	556	(30)
Tt WT	CO	423	567/541	(19)
Tt P115A		424	568/538	this work
Tt I5L		424	565/541	this work
Tt P115A/I5L		424	570/542	this work
Hb		419	569/540	(30)
Mb		423	579/542	(30)
Tt WT	NO	420	575/547	(19)
Tt P115A		418	573/543	this work
Tt I5L		421	572/539	this work
Tt P115A/I5L		421	568/535	this work
Hb		418	575/545	(30)
Mb		421	575/543	(30)
Tt WT	O₂	416	591/556	(19)
Tt P115A		416	584/548	this work
Tt I5L		418	587/550	this work
Tt P115A/I5L		417	588/552	this work
Hb		415	576/541	(30)
Mb		418	580/542	(30)

[a] All peak positions are reported in nm.

Table 2

Heme skeletal modes for the Fe^{II}-unligated and Fe^{II}-O_2 complexes of *Tt* H-NOX, hemoglobin, myoglobin, and FixL.[a]

Protein	Ligand	ν_{10}	ν_2	ν_3	ν_4	ν(Fe-X)	Ref.
Tt WT	unligated	1600	1565	1469	1353	217	(19)
Tt P115A		1602	1567	1469	1353	223	this work
Tt I5L		1599	1564	1469	1352	217	this work
Tt P115A/I5L		1601	1566	1471	1354	220	this work
Hb		nr[b]	1564	1470	1356	217	(35,36)
Mb		nr	1563	1471	1357	220	(35,36)
Bj FixLH[c]		1602	1555	1469	1353	218	(31)
Tt WT	O_2	1624	1579	1499	1375	567	(19)
Tt P115A		1631	1581	1503	1377	565	this work
Tt I5L		1627	1580	1499	1372	564	this work
Tt P115A/I5L		1630	1582	1502	1375	562	this work
Hb		nr	1581	1503	1376	570	this work
Mb		nr	1584	1506	1377	570	this work
Bj FixLH		1638	1579	1504	1377	569	(31)

[a] All vibrational frequencies are reported in cm^{-1}.

[b] nr = not reported.

[c] *B. japonicum* FixL heme-PAS.

Table 3

Calculated heme out-of-plane distortions from normal coordinate structural decomposition (NSD) analysis for the O_2 complex of Tt H-NOX and other heme proteins.

PDB	Protein	Δ_{oop} [a]	B_{2u} [b]	B_{1u}	A_{2u}	$E_{g(x)}$	$E_{g(y)}$	A_{1u}	Ref.
1U55	Tt WT A	1.59	−1.07	−1.11	−0.1	−0.10	0.24	−0.03	(14)
1U55	Tt WT B	1.11	−0.65	−0.79	0.32	−0.24	0.02	−0.03	(14)
1U4H	Tt WT A	1.59	−1.09	−1.09	−0.02	−0.30	0.11	−0.06	(14)
1U4H	Tt WT B	1.60	−1.00	−1.20	0.10	−0.15	0.14	−0.06	(14)
Heme A	Tt 15L	1.28	−0.93	0.73	−0.11	−0.18	0.40	−0.02	c
Heme B	Tt 15L	1.23	−0.81	−0.81	0.13	−0.31	0.14	−0.02	c
3EEE	Tt P115A A	0.90	−0.40	−0.77	0.04	−0.17	0.02	0.00	(20)
3EEE	Tt P115A B	0.82	−0.50	−0.61	0.03	−0.11	0.03	0.01	(20)
3EEE	Tt P115A C	0.54	−0.04	−0.49	−0.09	−0.16	−0.08	0.01	(20)
3EEE	Tt P115A D	0.62	0.07	−0.52	−0.03	−0.25	−0.18	0.01	(20)
Heme A	Tt 15L/P115A	0.85	−0.53	0.05	−0.16	−0.05	0.52	−0.04	c
Heme B	Tt 15L/P115A	0.74	−0.63	0.17	−0.02	0.01	0.32	−0.08	c
1DP6	Bj FixL [d]	0.60	0.44	−0.32	0.18	0.01	0.11	−0.03	(26)
1A6M	Sw Mb [e]	0.36	0.19	0.01	0.22	−0.05	0.19	0.07	(28)
1ASH	As Hb [f]	0.47	−0.11	0.41	0.08	−0.11	0.07	−0.01	(29)
1IDR	tHb A [g]	0.58	−0.13	0.33	0.28	−0.25	−0.19	0.04	(27)
1IDR	tHb B [g]	0.55	0.15	0.45	0.01	0.05	−0.21	−0.04	(27)

[a] Total out-of-plane displacement (Å) from the complete basis set

[b] Reported displacements for each symmetry type are from the minimal basis set

[c] unpublished experiments, Olea et al.

[d] O_2-sensing FixL domain of *Bradyrhizobium japonicum*

[e] Sperm whale myoglobin

[f] *Ascaris suum* hemoglobin domain I

[g] Truncated hemoglobin N from *Mycobacterium tuberculosis*